Radiative heat transfer modelling in a concentrated solar energy bubbling fluidized bed receiver using the Monte Carlo Method

Germain Baud, Jean-Jacques Bézian, Mouna El-Hafi, Gabriel Olalde

Radiative heat transfer modelling in a concentrated solar energy bubbling fluidized bed receiver using the Monte Carlo Method

Journal of Physics: Conference Series **369** (2012) 012030 doi:10.1088/1742-6596/369/1/012030

Radiative heat transfer modelling in a concentrated solar energy bubbling fluidized bed receiver using the Monte Carlo Method

Germain BAUD[1], Jean Jacques BEZIAN[1], Mouna EL HAFI[1] and Gabriel OLALDE[2]

1) Université de Toulouse; CNRS; Centre RAPSODEE, Ecole des Mines d'Albi, Albi, France
2) PROMES, CNRS, Odeillo, France

E-mail: mouna.elhafi@enstimac.fr

Abstract. According to recent studies in the solar energy community, a promising ways of solar energy conversion seems to be the beam down concentration technology associated to a fluidized bed receiver. The advantage of this system is its ability to heat air at temperature reaching 1000 K in a receiver directly exposed to a concentrated solar beam and integrated in a thermodynamic cycle. This paper focus on the modelling of radiative heat transfer from the optical concentrator to the receiver by taking into account absorption and multiple scattering of light in the particles bed. To achieve this objective, we develop in this work an efficient tool based on an algorithm solving the integral formulation of the Radiative Transfer Equation by the Monte Carlo Method. This algorithm is implemented in EDStaR environment where computer graphics libraries, parallel computing and specific functionalities to produce statistical quantities and their associated derivatives are available. One of the main advantage of the proposed radiative transfer modelling is the determination of the sensitivities (derivatives) of the physical quantities to any physical or geometrical parameter without significant additional CPU time.

1. Introduction

Fluidized beds are conventionally used as media of thermal exchanges for high temperature processes because of their excellent performance in terms of heat transfer. To improve the performance of thermodynamic cycles for solar electricity production, a technological gap will be the direct gas heating in solar receiver, to obtain at the entrance of a turbine temperatures at a level higher than 1000 K. One of the best solutions would be to use solid particles in a fluidized bed directly submitted to the concentrated solar flux (see fig.1.b). The main advantages of the fluidized bed receiver are its thermal efficiency, an improved resistance to thermal stress compared to metallic and ceramic receivers and its adaptability with beam down concentrators allowing to produce electricity directly on the ground. For these reasons, fluidized bed solar receivers and reactors have been designed and studied by numerous scientists [1, 2, 3, 4].

To evaluate the efficiency of these solar receivers, we need to determine the heat losses caused by radiation which becomes the major mechanism for heat transfer losses from the receiver. The accuracy and the power level of the flux map obtained at the surface of the receiver depends on many optical parameter such as the reflectivity or the quality of the mirrors, the design of the concentrators, etc. The optical and geometrical design of such systems require powerful

tools to provide radiative heat transfer exchanges inside the receiver and also to compute the distribution of the irradiation on the receiver.

In this context, several softwares have been developed such as Mirval [5], Soltrace [6], Stral [7] and Tonatiuh [8, 9]. They commonly use the Monte Carlo ray-tracing to predict the concentrated solar flux distribution incident on a receiver [10]. In this method, solar radiation is assumed to be composed of discrete energy bundles and the computation consists of following their probable paths that are generated randomly from the solar source to the optical components. Steinfeld and co-workers have also developed Monte Carlo ray-tracing in-house codes to compute the distribution of solar irradiation on receiver boundaries [11, 12, 13, 14]. Most of the time, these existing tools allow to design the optical part of the concentrated solar system only. What we propose in this study is to model radiation in the whole system: the concentrated solar source from the optical device and the absorption by particles inside the solar receiver. The aim of this study is to calculate the penetration of the incident solar beams through the window (see. fig.1.a) and to estimate the radiative heat loss by reflection. We need for that a radiative model to calculate the absorbed and scattered radiative contribution by particles inside the receiver. Knowing this radiative contribution, the energy balance could be performed and the heat exchange between air and particles could be evaluated.

In this work, the Radiative Transfer Equation (RTE) is solved through its integral formulation. The Monte Carlo Method (MCM) in this case is used as a numerical method to calculate explicitly these integrals. As it is explained in previous studies [16], the main advantage of this integral formulation is to analyse physically the radiative exchanges but also to calculate physical quantities such as radiative fluxes, radiative source terms with their associated sensitivities to any parameter, without additional CPU time.

A first part is dedicated to the description of the radiative properties of particles. Then, the radiative model is presented. The associated algorithm using MCM is detailed determining the radiative heat loss with the multiple scattering by particles and reflection by the walls. An illustration of sensitivity calculation by MCM is shown.

2. The system under investigation

In this work, we model a 45 cm high solar receiver consisting of a diffuser at the bottom of a lower cylindrical column mesuring 25x7 cm, a medium conical part of 7.5 cm high and an upper part of 12.5x12 cm surmounted by a quartz window (see fig.1.a). The concentrated solar radiation enters the top of the receiver and is directly absorpted by the fluidized particles of silicon carbide. The solar receiver allows us to heat the gas sent through the metallic diffuser at the bottom of the column. Air mass flow must reach a threshold to support a good fluidisation of solid particles to maximise heat exchanges and solar radiation depth of penetration. The rise of diameter in the middle of the receiver prevent particles from exiting the fluidisation column or impacting the window.

The present receiver is coupled with a beam-down concentrator available in the laboratory of PROMES, Odeillo, France (see fig.1.b). This system is constituted by a flat heliostat reflecting solar energy to a dish with a diameter of 4.6 m, a focal length of 3.9 m and a focal spot of approximatively 6 cm.

A laboratory scale set-up of this receiver have been studied in the PhD thesis of A.Bounaceur [17]. According to this work, it was possible to heat air from the ambient temperature up to 930 K with a thermal efficiency of 70%. But as discussed in this work, even better results could be reached by reducing radiative losses and avoiding the overheating of the walls of the receiver.

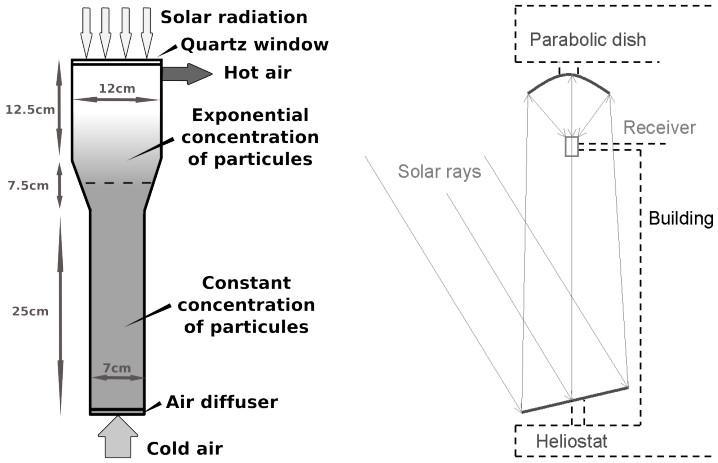

Figure 1. Scheme of the solar fluidized bed receiver on the left (a). Scheme of the Beam down solar concentrator on the right (b).

3. Modelling of radiative heat transfer

3.1. Radiative properties

The stainless steel surface of the receiver ($\mathcal{R}$) is represented by a diffuse-reflective surface with a grey reflectivity $\rho^{\mathcal{R}}$. The quartz window ($\mathcal{G}$) is considered as a specularly diffuse and transmittive surface with a reflectivity $\rho^{\mathcal{G}}(\omega, \mathbf{n})$.

When the particle bed is submitted to radiation, the mechanisms responsible for the distribution of light are absorption and scattering. The spread of radiation occurs through the interstices of the particle fluidized bed and by transmission and scattering through the particles. The air is considered transparent. The length of penetration of radiation depends largely on the receiver geometry, the volumetric fraction of the fluidized bed and the optical properties of particles. Absorption and scattering coefficients in the fluidized bed derive from density and optical properties of particles. The phase function describing scattering in the particle cloud is modelled by the Henyey-Greenstein phase function.

To determine the optical properties of the particles, a calculation over the whole solar spectrum between 0.24 μm and 4 μm is processed using a code developed by Mishchenko based on the Mie theory [19], where the index of refraction is 0.78. Preliminary results [18] have shown that spectral resolution make no significant difference compared to wavelength-integrated calculations when computing the flux in a SiC fluidized bed. Thus, incoming solar radiation is considered monochromatic and we average the values of optical properties Q_s, Q_a and g from the spectral absorption and scattering efficiency factors $Q_{\nu,s}$, $Q_{\nu,a}$ and the asymmetry factor g_ν. The optical properties are described by the following values of the absorption and scattering cross sections :

$$\sigma_a = \frac{Q_a}{\pi d_p^2/4} \quad ; \quad \sigma_s = \frac{Q_s}{\pi d_p^2/4} \tag{1}$$

with $Q_s = 1.51$, $Q_a = 0.5$, $g = 0.7$ and the particle diameter d_p.
Absorption and scattering coefficients are calculated from cross sections and density through :

$$k_a = \eta(\mathbf{x}, p)\sigma_a \quad ; \quad k_s = \eta(\mathbf{x}, p)\sigma_s \tag{2}$$

The determination of the distribution of particles within the fluidized bed has been a critical parameter for the calculation of heat transfer. According to our experimental observations, the receiver can be divided in two parts : (i) the bottom part of the bed within which the particle concentration is constant and high, (ii) the upper part of the bed, within which the particle

concentration can be conceptualized by a exponential decay (see fig.1.a). The exponential density of particles from the upper part of the receiver is thus described by :

$$\eta(\mathbf{x}, p) = \eta_0 exp(-\frac{z - z_0}{p}) \tag{3}$$

with η_0 the density in the constant zone, z the height in the fluidized bed, z_0 the height indicating the change from a constant to an exponential density and p a parameter tuning the exponential distribution.

3.2. Method of modelling and algorithm : Calculation of reflection losses

Our concern is to describe in detail the calculation of the fraction of radiative power exiting through the window without being absorbed by the receiver and to compute the sensitivity of this loss to the p parameter of the density of particle. The solar radiation is considered collimated. The algorithm allowing us to calculate this value is the following :

- Uniform drawing of a point x_0 on the window, according to the density probability function $p_{x_0} = 1/S_{\mathcal{G}}$;
- Emission of a photon bundle from the point x_0 in the normal direction to the surface $\omega_0 = n_{x_0}$;
- Drawing of a first optical thickness κ_0 according to the law $p_{\kappa_0}(\kappa_0) = exp(-\kappa_0)$ if the bundle is in the bottom dense zone of the receiver and $p_{\kappa_0}(\kappa_0) = exp(-\kappa_0)/(1 - exp(-\kappa_{max}))$ if the bundle is in the upper zone of the receiver ;
- *Interaction* - If κ_j is smaller than κ_p the optical thickness of the optical path travelled by the photon bundle until its next interaction with the boundaries of the receiver, then the interaction point $x_j(x_{j-1}, \omega_{j-1})$ belongs to the volume of the receiver. If κ_j is bigger than κ_p, then x_j belongs to the surface ($\mathcal{R}$) or the windows ($\mathcal{G}$) ;
- *reflection on the surface of the receiver* - If $x_j \in \mathcal{R}$ and $\hat{w}_j \geq \epsilon$, then we draw one reflection direction ω_{j+1} according to the lambertian law. We also reduce the energy of the photon bundle by $exp(-\kappa_a)$ the absorption of the cloud of particle among the optical path and $\rho^{\mathcal{R}}$ the reflectivity of the surface ;
- *reflection on the surface of the receiver, Russian roulette mode* - If $x_j \in \mathcal{R}$ and $\hat{w}_j < \epsilon$, then we draw a number $r_{j+1} \in [0, 1]$. If r_{j+1} is smaller than $\rho^{\mathcal{R}}$, then the photon bundle continue its path (drawing of a reflection angle, drawing of a new optical thickness...). Otherwise, the photon bundle stops its path, and its weight is void ;
- *Interaction with the windows* - If $x_j \in \mathcal{G}$, then we draw a number $r_{j+1} \in [0, 1]$. If r_{j+1} is smaller than $\rho^{\mathcal{G}}$, then the photon bundle continue its path (drawing of a reflection angle, drawing of a new optical thickness...). Otherwise, the photon bundle exits the receiver : the algorithm comes to an end and it process to the calculation of the weights of E and its sensitivity;
- *Scattering in the volume* - If $x_j \in \mathcal{V}$, then we draw a direction of scattering ω_{j+1} according to the phase function. Then we reduce the energy of the photon bundle by $exp(-\kappa_j)$ the absorption of the cloud of particle among the optical path and continue the optical path of the photon bundle (drawing of a reflection angle, drawing of a new optical thickness...) ;
- *Calculation of $\hat{w}_j$, the weight of E* - Physically, the weight is the product of the area of the emitting surface $S_{\mathcal{G}}$ by the attenuation of the energy of the photon bundle through its path among the receiver. The extenuation is due to both the absorption from the impacts with the surface of the receiver and the absoprtion of the participating medium ;

- *Calculation of $\hat{w}_{p,j}$, the weight of the sensitivity of E to parameter p* - The expression of the weight of $\frac{\partial E}{\partial p}$ is a little more complicated than the one of the weight of E, but it can be processed at the same time and with the same algorithm.

A "Russian roulette" has been implemented to deal with the reflection at the boundaries of the receiver when the weight become smaller than a certain criterion. Doing so, the computer time necessary for one computation is reduced from 1 hour to a few minutes. The reason why a calculation could take so much time is that the bottom of the bed contains a high particle density and thus the scattering and absorption mean free path are very small in this zone. Consequently, a ray entering this zone will encounters a large number of scattering events before it exits from the receiver by the window. In the meanwhile, the extinction contribution becomes higher and the energy decreases quickly. So, when performing a calculation, the dedicated computing time to multiple scattering of paths with very low energy (ie. low weight) remains significant.

With the "Russian roulette", when the energy of a ray is lower than a defined value, we do not treat the reflection as a ray being reflected and attenuated by the surface, but we test if the interaction point is an absorption or a reflection. When the interaction is a reflection, we process until the next interaction. If the interaction is an absorption, the optical path dies.

This algorithm is implemented in the environment EDStaR which is constituted by an advanced technology allowing the modelling of corpuscular transport and in particular radiative transfer focusing on the Monte Carlo Method. EDStaR is not a code, but rather a development environment providing a library of useful functions to deal with parallel calculation, calculation of sensitivities, ray tracing in complex 3D geometries using computer graphics libraries [21]. More informations about EDStaR are available on line at the following url : http://wiki-energetique.laplace.univ-tlse.fr/wiki/index.php/Edstar.

The integral formulation of the Monte Carlo algorithm described above can be written as follow. Using the same notations as previously, the fraction of the radiative power E exiting through the quartz window is :

$$E = \int_{\mathcal{G}} p_{\mathbf{X}_0}(\mathbf{x}_0) d\mathbf{x}_0 \int_0^\infty p_{\kappa_0}(\kappa_0) d\kappa_0 \left\{ \begin{array}{l} H(\mathbf{x}_1 \in \mathcal{R}) \int_{2\pi} p^{\mathcal{R}}_{\mathbf{\Omega}_1}(\omega_1) d\omega_1 \int_0^\infty p_{\kappa_1}(\kappa_1) d\kappa_1 \; \mathcal{I}_1 \\ +H(\mathbf{x}_1 \in \mathcal{V}) \int_{4\pi} p^{\mathcal{V}}_{\mathbf{\Omega}_1}(\omega_1|\omega_0) d\omega_1 \int_0^\infty p_{\kappa_1}(\kappa_1) d\kappa_1 \; \mathcal{I}_1 \end{array} \right\} \quad (4)$$

where $\mathcal{I}_j, j > 1$ is recursively defined as

$$\begin{array}{rl} \mathcal{I}_j & = H(\mathbf{x}_{j+1} \in \mathcal{G}) \int_0^1 p_{R^{\mathcal{G}}_{j+1}}(r^{\mathcal{G}}_{j+1}) dr^{\mathcal{G}}_{j+1} \times ... \\ & \left\{ \begin{array}{l} H(r^{\mathcal{G}}_{j+1} > \rho^{\mathcal{G}}) \; \hat{w}_{j+1} \\ +H(r^{\mathcal{G}}_{j+1} \leq \rho^{\mathcal{G}}) \int_{2\pi} p^{\mathcal{G}}_{\mathbf{\Omega}_{j+1}}(\omega_{j+1}|\omega_j) d\omega_{j+1} \int_0^\infty p_{\kappa_{j+1}}(\kappa_{j+1}) d\kappa_{j+1} \; \mathcal{I}_{j+1} \end{array} \right\} \\ & +H(\mathbf{x}_{j+1} \in \mathcal{R}) \left\{ \begin{array}{l} H(\hat{w}_j \leq \epsilon) \int_0^1 p_{R^{\mathcal{R}}_{j+1}}(r^{\mathcal{R}}_{j+1}) dr^{\mathcal{R}}_{j+1} \times ... \\ \left\{ \begin{array}{l} H(r^{\mathcal{R}}_{j+1} > \rho^{\mathcal{R}}) \times 0 \\ +H(r^{\mathcal{R}}_{j+1} \leq \rho^{\mathcal{R}}) \int_{2\pi} p^{\mathcal{R}}_{\mathbf{\Omega}_{j+1}}(\omega_{j+1}) d\omega_{j+1} \int_0^\infty p_{\kappa_{j+1}}(\kappa_{j+1}) d\kappa_{j+1} \; \mathcal{I}_{j+1} \end{array} \right\} \\ +H(\hat{w}_j > \epsilon) \int_{2\pi} p^{\mathcal{R}}_{\mathbf{\Omega}_{j+1}}(\omega_{j+1}) d\omega_{j+1} \int_0^\infty p_{\kappa_{j+1}}(\kappa_{j+1}) d\kappa_{j+1} \; \mathcal{I}_{j+1} \end{array} \right\} \\ & +H(\mathbf{x}_{j+1} \in \mathcal{V}) \int_{4\pi} p^{\mathcal{V}}_{\mathbf{\Omega}_{j+1}}(\omega_{j+1}|\omega_j) d\omega_{j+1} \int_0^\infty p_{\kappa_{j+1}}(\kappa_{j+1}) d\kappa_{j+1} \; \mathcal{I}_{j+1} \end{array} \quad (5)$$

Where the various angle probability density functions are :

$$\begin{array}{l} p^{\mathcal{R}}_{\mathbf{\Omega}_j}(\omega_j) = \frac{\omega_j . \mathbf{n}_j}{\pi} \\ p^{\mathcal{V}}_{\mathbf{\Omega}_j}(\omega_{j+1}|\omega_j) = \frac{1-g^2}{[1+g^2-2g(\omega_{j-1}.\omega_j)]^{3/2}} \\ p^{\mathcal{G}}_{\mathbf{\Omega}_j}(\omega_{j+1}|\omega_j) = \delta(\omega_{j+1}.t_j + \omega_j.t_j)\delta(\omega_{j+1}.n_j - \omega_j.n_j) \end{array} \quad (6)$$

with n_j and t_j are respectively the normal vector and a tangent vector to the considered surface at the point x_j. And where the optical thickness probability density function is :

$$\kappa_j = \int_0^{||x'-x_j||} k_s(x_j + s\omega_j)ds \tag{7}$$

with $x_j = x'$ if $\kappa_j < \int_0^{||x_j-y_j||} k_s ds$ and $x_j = y_j$ if $\kappa_j \geq \int_0^{||x_j-y_j||} k_s ds$, $\omega_0 = n_{x_0}$ and $x' = x_j + ||x' - x_j||\omega_j$.

The weight is then recursively defined as

$$\hat{w}_{j+1} = \hat{w}_j exp(-\sigma_a \alpha_j) \left\{ \begin{array}{l} H(\mathbf{x}_{j+1} \in \mathcal{G}) \times 1 \\ +H(\mathbf{x}_1 \in \mathcal{R}) \left\{ \begin{array}{l} H(\hat{w}_j > \epsilon)\rho^{\mathcal{R}} \\ +H(\hat{w}_j \leq \epsilon) \times 1 \end{array} \right\} \\ +H(\mathbf{x}_1 \in \mathcal{V}) \times 1 \end{array} \right\} \tag{8}$$

with $\hat{w}_0 = S_{\mathcal{G}}$ and

$$\alpha_j = \int_0^{||\mathbf{x}_{j+1}-\mathbf{x}_j||} \eta(\mathbf{x}_j + s\omega_j, p)ds \tag{9}$$

In the particular case of a uniform particle density $\sigma_a \sum_{q=0}^{j-1} \alpha_q = \sigma_a \eta d_j = k_a d_j$ and the integral formulation corresponding to the sensitivity $\frac{\partial E}{\partial \eta}$ is identical to that of E in Eqs. 4 and 5, replacing only $\hat{w}_j$ with

$$\hat{w}_{\eta,j} = \frac{\partial \hat{w}_j}{\partial \eta} + \hat{w}_j \sum_{q=0}^{j-1} \frac{\frac{\partial p_{\lambda_q}}{\partial \eta}}{p_{\lambda_q}} = \hat{w}_j \left[-\sigma_a d_j + \sum_{q=0}^{j-1} \frac{1-\kappa_q}{\eta} \right] \tag{10}$$

In the general case, the integral formulation corresponding to the sensitivity $\frac{\partial E}{\partial p}$ is identical to that of E, replacing only $\hat{w}_j$ with

$$\hat{w}_{p,j} = \hat{w}_j \sum_{q=0}^{j-1} \left[-\sigma_a \frac{\partial \alpha_q}{\partial p} - \sigma_s \frac{\int_0^{||\mathbf{x}'-\mathbf{x}_q||} \eta(\mathbf{x}_q + s\omega_q, p)ds}{\partial p} + \frac{\partial_2 \eta(\mathbf{x}_{q+1}, p)}{\eta(\mathbf{x}_{q+1}, p)} \right] \tag{11}$$

where $\partial_2 \eta(\mathbf{x}, p)$ is the partial derivative with p of η.

As the expression of the sensitivity is not correlated with the density profile outside of the receiver, we can choose by convention that κ_j does not depend on $\eta(\mathbf{x}, p)$ and that $\partial_2 \eta(\mathbf{x}_{q+1}, p) = 0$ when $\mathbf{x}_{q+1} \notin \mathcal{V}$ (when reflection occurs before scattering). As a result, we have :

$$\begin{aligned} \int_0^{||\mathbf{x}'-\mathbf{x}_q||} \eta(\mathbf{x}_q + s\omega_q, p)ds &= \int_0^{||\mathbf{x_{q+1}}-\mathbf{x}_q||} \eta(\mathbf{x}_q + s\omega_q, p)ds + \int_0^{||\mathbf{x}'-\mathbf{x_{q+1}}||} \eta(\mathbf{x}_q + s\omega_q, p)ds \\ &= \int_0^{||\mathbf{x_{q+1}}-\mathbf{x}_q||} \eta(\mathbf{x}_q + s\omega_q, p)ds \end{aligned}$$

and the sensitivity becomes :

$$\hat{w}_{p,j} = \hat{w}_j \sum_{q=0}^{j-1} \left[-(\sigma_a + \sigma_s) \frac{\partial \alpha_q}{\partial p} + H(x_{q+1} \in \mathcal{V}) \frac{\partial_2 \eta(\mathbf{x}_{q+1}, p)}{\eta(\mathbf{x}_{q+1}, p)} \right] \tag{12}$$

3.3. Modelling of the concentrator and optical errors

In the description above, for didactic purpose, the solar radiation have been considered collimated. In our case study, the incoming concentrated solar radiation reaching the receiver is focalized. To model such systems, a beam-down like concentrator as been implemented in the previous code featuring a dish focalizing solar energy from infinity to the receiver.

As no concentrator is perfect, we take into account the misalignment of the heliostat, the surface structural defects of the mirrors, and the sunspot effect, by including a statistical error when tracing the reflection angle on the surface of the dish. Our model is inspired by Blinn [21] in order to render rough shiny materials in physically based picture rendering.

As a theoretical reflected ray is reflected specularly with the normal vector to the surface n_j as a reference, the imperfect reflected ray is traced using a modified normal vector n_h. In practical terms, the modified normal vector is drawn inside of a cone centered on the normal vector to the surface, following the probability density function :

$$P_{n_h}(n_h|\omega_j;p) = \frac{2+1/e}{2\pi(1-cos(\frac{\pi}{4}-\frac{1}{2}arccos(\omega_j.n_{j+1})))^{2+1/e}}(n_h.n_{j+1})^{1+1/e} \tag{13}$$

Using the experimental map flux taken at the focus point of a real concentrator, the parameter e of the model is adjusted. Figure 2.b shows the comparison between experimental [20] and adjusted numerical map flux taken at the focus point of the concentrator.

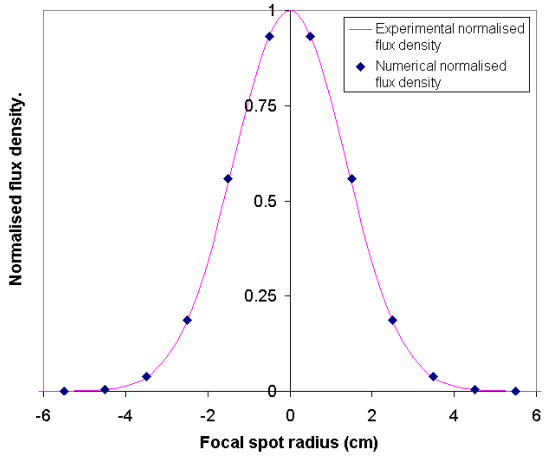

Figure 2. Scheme of the beam-down solar concentrator of Odeillo, France (a). Experimental [20] and adjusted numerical map flux taken at the focus point of the concentrator (b).

4. Results : Calculation of reflection losses and its sensitivity analysis

4.1. Validation of the sensitivity calculation in the case of collimated light

The radiative power exiting the receiver without being absorbed (see fig.3) and its sensitivity to the parameter p specifying the exponential decrease of the density of particles (see fig.4) are computed using a reflectivity of the stainless steel surface of the receiver of $\rho^{\mathcal{R}}$=0.4 and a reflectivity of the quartz window ($\mathcal{G}$) of $\rho^{\mathcal{G}}$=0.1. The diameter of particule and the density of particles in the constant zone are chosen such as d_p =280 μm and $\eta_0 = 26.10^3$ cm^{-3}.

The average computer time for a run of 10^6 realizations as used in the results shown in figure 3 is about a few minutes on a AMD Opteron Processor 246 with 2Gb ram.

Comparing the value of the fraction of losses and its sensitivity to p, we can minimize the energy losses by choosing p around 0.014. As p parameter increases over 0.014, the concentration of particles in the upper part of the fluidized bed decreases and the solar radiation have a higher probability to reach the stainless steel surface of the choke point and to be reflected outside of

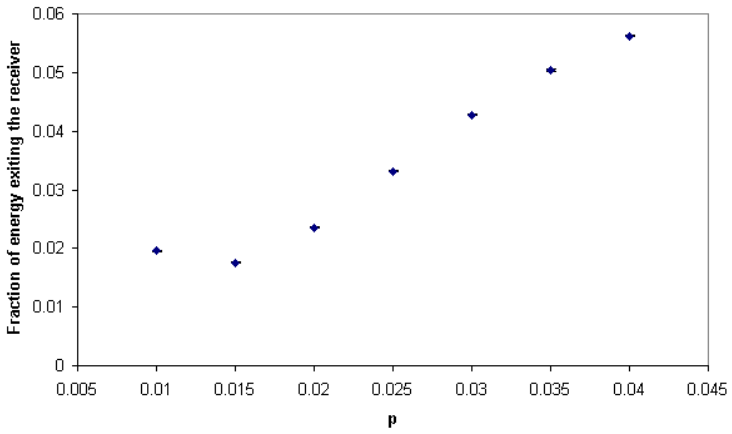

Figure 3. Fraction of incoming energy that exit the receiver without being absorbed, the p parameter of the density of particle is fixed. Error bars corresponding to the estimated standard deviation of the Monte Carlo Method are less than 1%.

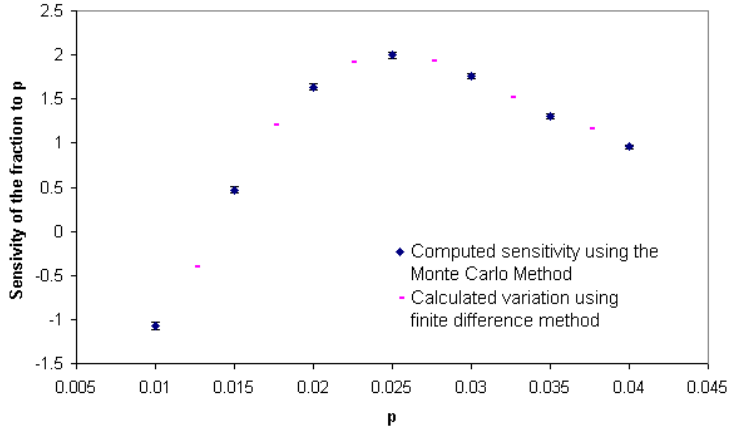

Figure 4. Sensitivity of the exiting fraction to p calculated by both the MCM and the finite difference method as reference, p is fixed. Error bars corresponding to the estimated standard deviation of the Monte Carlo Method are negligible.

the receiver. On the contrary, when p decreases below the value of 0.014, we notice that the losses increase again. Indeed since the energy refracted by the particles becomes predominant when high particle density move closer to the top of the receiver.

4.2. Fraction of losses and its sensitivity calculation to p

For different concentrator / receiver layouts, the data of table 1 represent incoming solar radiation losses. The different layouts of the receiver that have been moved in a range of 100 mm to allow the focus plan of the concentrator to move in a range of 50 mm at the front and rear of the quartz window of the fluidized bed receiver (see fig.5). For each test, the losses are obtained for the optimal value of parameter p, found using the sensitivity calculations.

Table 1. Visible radiative losses for different concentrator/receiver layouts

	Case 1	**Case 2**	**Case 3**	**Case 4**
Incoming radiation	collimated	focused	focused	focused
Focal point position/window (mm)	x	0	-50	+50
Optimal p parameter	0.014	0.018	0.015	0.027
Aiming losses (%)	0	0	1.17	1.16
Window reflection losses (%)	3.47	5.35	5.31	5.24
Bed reflection losses (%)	1.7	3.08	1.89	5.24
Total losses (%)	5.17	8.43	8.37	12.09

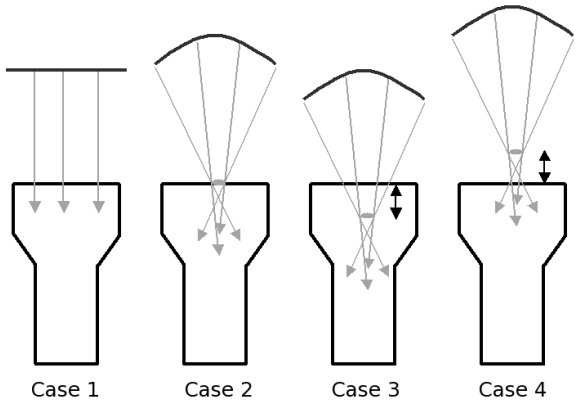

Figure 5. The four cases studied corresponding to different concentrator / receiver layouts

According to the results, we notice that reflection of the window is the main source of radiative heat loss. Even if the total losses reach the maximum when the focus point of the concentrator is located outside the receiver, we point out that for each receiver position, a specific value of parameter p can be found in order to reduce the bed reflection losses. In other words, it implies that the control of the particle distribution produced by the fluidisation inside the receiver must be adjusted according to the incoming solar radiation.

5. Conclusion

We presented in this study an original radiative transfer model that allows us to calculate the propagation of light from a beam-down concentrator to a fluidized bed receiver, taking into account the multiple scattering of light in the particulate medium and the directionality of the concentrated solar radiation. Our approach is based on the integral formulation of the RTE solved by the MCM. The algorithm is implemented in a new environment EDStaR, allowing the convenient implementation of an in house radiative model and the calculation of parametric sensitivities with nearly no additional CPU cost. To illustrate this approach, we studied the effect of the concentration of particles of a fluidized bed receiver on radiative loss by reflection. This information can be useful in order to maximise the efficiency of the receiver. As infra red radiative losses can reach 30% of the global losses of the receiver, the next step is to apply this method to model infra red radiative transfer in the fluidized bed receiver.

Nomenclature

Greek letters

α, β	limits of integration
η	concentration of particles, m^{-3}
κ	optical thickness, m^{-1}
ω, Ω	angle of emission
ϕ	flux density, W/m^2
ρ	Reflectivity
σ	cross section, m^2
σ^2	variance

Subscripts

0	(subscript) initial
$\mathcal{G}$	(subscript) window
$\mathcal{R}$	(subscript) wall
$\mathcal{V}$	(subscript) volume
a	(subscript) absorption
i, j, q	(subscript) indexes
p	(subscript) particle
s	(subscript) scattering

Symbols

d	diameter, m
E	radiative power exiting fraction, %
e	parameter describing the modified normal vector drawing probability density function
g	asymmetry factor

H	Heavy side function	Q	efficiency factor
I	integral, recursive term	r	random number in [0,1]
l	length of the path between two interactions	S	area, m^2
N	number of realizations	t	tangent vector to the surface
n	normal vector to the surface	x	variable, position, interaction position
p	parameter describing the exponential decay of particles	y	interaction point with a boundary
$P(x)$	density probability function	z	height, m
		$\hat{w}$	weight

References

[1] Flamant G. and Menigault T., 1986. Combined wall-to-fluidized bed heat transfer. Bubbles and emulsion contributions at high temperature, Int. J. Heat Mass Transfer, 30, 9, 1803-1812.
[2] Haddad I. M. and Elsayed M. M., 1988. Transient performance fluidised bed solar receiver at various parametric conditions, Solar and Wind Technology Journal., Vol. 5, No. 6, pp 653-659.
[3] Muller. R., Zedtwitz P. V., Wokaun A. and Steinfeld A., 2003. Kinetic investigation on steam gasification of charcoal under direct high-flux irradiation, Chem. Engin. Sci. No. 58, pp. 5111-5119.
[4] Trommer D. and al., 2005. Hydrogen production by steam-gasification of petroleum coke using concentrated solar power: Thermodynamic and Kinetic analyses, Int. Journal of Hydrogen Energy. No. 30, pp. 605-618.
[5] Leary, P.L., Hankins, J.D., 1979. Users guide for MIRVAL: a computer code for comparing designs of heliostat-receiver optics for central receiver solar power plants, Sandia Report SAND-77-8280.
[6] Wendelin, T., 2003. SolTRACE: a new optical modeling tool for concentrating solar optics, in: Proceedings of the ISEC 2003: International Solar Energy Conference, 15-18 March 2003, Kohala Coast, Hawaii, New York, American Society of Mechanical Engineers, pp. 253-260.
[7] Belhomme B., Pitz-Paal R., Schwarzbzl P., Ulmer S., 2009. A new fast ray tracing tool for high-precision simulation of heliostat fields. ASME Journal of Solar Energy Engineering 131(3), 031002.
[8] Blanco M.J., Mutuberria A., Garcia P., Gastesi R., Martin V., 2009. Preliminary validation of Tonatiuh, in: Proceedings of the International Energy Agency's SolarPACES Symposium 2009,
[9] Blanco M.J., Amieva J., Mancilla A., 2005. The Tonatiuh Software Development Project: An Open Source Approach to the Simulation of Solar Concentrating Systems, in: Proceedings of 2005 ASME IMEC: 2005 ASME International Mechanical Engineering Congress & Exposition, Orlando, Florida.
[10] Garcia P., Ferriere A., Bezian J.-J., 2007. Codes for solar flux calculation dedicated to central receiver system application: a comparative review, Solar Energy 82(3), 189-197.
[11] Lipinski W., Steinfeld A., 2004. Heterogeneous thermochemical decomposition under direct irradiation. International Journal of Heat and Mass Transfer 47, 1907-1916.
[12] Muller R., Steinfeld A., 2007. Band-approximated radiative heat transfer analysis of a solar chemical reactor for the thermal dissociation of zinc oxide. Solar Energy 81(10), 1285-1294.
[13] Petrasch J., Steinfeld A., 2007. Dynamics of a solar thermochemical reactor for steam-reforming of methane. Chemical Engineering Science 62(16), 4214-4228.
[14] Muller R., Lipinski W., Steinfeld A., 2008. Transient heat transfer in a directly-irradiated solar chemical reactor for the thermal dissociation of ZnO. Applied Thermal Engineering 28, 524-531.
[15] Roger, M. 2006. Modeles de sensibilite dans le cadre de la methode de Monte-Carlo : Illustrations en transfert radiatif, 24 mai 2006, Institut National Polytechnique de Toulouse, PhD thesis.
[16] Bounaceur A., 2008. Interaction lit fluidise de particules solides-rayonnement solaire concentre pour la mise au point d'un procede de chauffage de gaz a plus de 1000K, PhD Thesis, Ecole des Mines de Paris.
[17] Baud G., 2011. Conception de recepteurs solaires a lit fluidise sous flux radiatif concentre, PhD Thesis, Institut National Polytechnique de Toulouse.
[18] Mie G., 1908. Beitrage zur optik truber medien spiezell kolloidallen metallosungen, Ann. d. physik, 25, 377-445.
[19] Flamant G., 1982. Theoretical and experimental study of radiant heat transfer in a solar fluidized bed receiver, AIChE Journal, Vol. 28, No. 4, pp. 529-535
[20] Pharr M., Humphreys G., 2004. Physically based rendering : from theory to implementation, Elvesier.
[21] Bezian JJ., Bounaceur A., De Ryck A., El Hafi M., 2007. Un nouveau concept de centrale solaire thermodynamique base sur un recepteur a lit fluidise, In : Actes des Journees Internationales de Thermique, Albi, FRANCE, ISBN 978-2-95-11591-6-7, p. 346-350